photonics

MDPI

Article

The Orbital-Resolved Dissociative Ionization of the Molecular IBr in a Near-Infrared Femtosecond Laser Field

Botong Liu [1,*] and Zhipeng Li [2]

[1] School of Information Engineering, Yancheng Institute of Technology, Yancheng 224051, China
[2] State Key Laboratory of Precision Spectroscopy, School of Physics and Electronic Science, East China Normal University, Shanghai 200062, China; 15201715520@163.com
* Correspondence: liubot@ycit.edu.cn

Abstract: The dissociative ionization of molecular IBr in a near-infrared femtosecond laser field was investigated through the utilization of the DC-sliced ion imaging technique. Two pathways, denoted as $(1, 0)^a$ and $(1, 0)^b$, were observed in the dissociation process of IBr^+ into an I^+ ion and Br atom. The distinct angular distributions observed in these pathways were found to be a result of the removal of electrons from different molecular orbitals. Specifically, in pathway $(1, 0)^a$, the electron was stripped from HOMO and HOMO-1, while in pathway $(1, 0)^b$, the electron was removed from HOMO-2. The ultrafast dynamical processes of molecules influenced by intense femtosecond laser fields were investigated through an analysis of the angular distribution characteristics of fragment ions in conjunction with the spatial properties of molecular orbitals.

Keywords: dissociative ionization; femtosecond laser; multi-orbital effect

1. Introduction

The development of ultrafast laser technology has made it a powerful tool for studying ultrafast dynamical processes of atoms and molecules. During the interaction between a laser and matter, ionization emerges as the primary physical phenomenon [1–4]. At sufficiently high laser intensities, atoms or molecules may undergo electron loss via multiphoton ionization and above-threshold ionization (MPI/ATI), despite the fact that the energy of a single photon is lower than the ionization potential (IP). The laser field modifies the internal potential barrier, thereby affecting the Coulomb potential between the nucleus and the electron as laser intensity increases. The electron may overcome this barrier and transition to a continuum state via tunneling ionization (TI). As laser intensity continues to rise, the internal potential barrier can be entirely below the energy level of the electron, thereby facilitating the removal of the electron, a process referred to as over-the-barrier ionization (OTBI). In the femtosecond laser field, ionization is widely acknowledged as the initial phase that occurs prior to dissociation processes in molecules, a phenomenon referred to as dissociative ionization (DI). When laser intensities exceed 10^{14} W/cm^2, the occurrence of multi-electron dissociative ionization (MEDI) becomes feasible. This process leads to the cleavage of chemical bonds within molecules, driven by the internal Coulomb repulsive energy associated with the multi-charged parent ions, a phenomenon commonly referred to as Coulomb explosion (CE) [5–8]. By analyzing the parameters of fragment products, such as momentum distribution, kinetic energy release (KER), and angular distribution, we can offer detailed insights into the dynamical processes of ionization and dissociation [9–11].

In the past decades, many studies have been focused on the coherent control over the photo-dissociation of IBr molecules. Chan et al. describe in detail a (ω1–ω3) path through the simultaneous excitation of a molecule that can significantly change the yield of IBr photo-dissociation products by adjusting the relative phase and intensity of the laser light, providing a new pathway for the precise control of chemical reactions at the molecular level through interference effects [12]. Jung et al. investigated the photo-dissociation of

check for updates

Citation: Liu, B.; Li, Z. The Orbital-Resolved Dissociative Ionization of the Molecular IBr in a Near-Infrared Femtosecond Laser Field. *Photonics* **2024**, *11*, 810. https://doi.org/10.3390/photonics11090810

Received: 8 July 2024
Revised: 11 August 2024
Accepted: 28 August 2024
Published: 29 August 2024

IBr at 304 nm and showed that the photo-dissociation of IBr molecules involves multiple electronic states and that the kinetic energy distribution of the dissociation products has a specific polarization dependence [13]. Lu et al. revealed that the yield of Br*/(Br + Br*) can be modulated by adjusting the relative phase and intensity ratio of the laser, thereby introducing a novel approach for the precise manipulation of chemical reactions [14]. Wrede et al. explored the photo-dissociation of the IBr molecule within the wavelength range of 440–685 nm utilizing high-resolution ion imaging. Their research not only elucidated the excited-state potential energy profile of the IBr molecule but also quantified the coupling strengths between the B and Y states [15]. Ohmura et al. implemented phase-controllable two-color laser pulses (ω–2ω) to achieve coherent control over the dissociative ionization process, facilitating molecular orientation solely through the laser field [16]. Most studies on the interaction of IBr with laser fields have used UV nanosecond laser fields. Therefore, the study of dissociative ionization of IBr in an 800 nm femtosecond laser field can fill this research gap and thus reveal the behavior and dynamics process of the molecule in a strong field.

In this research, we employ the DC-sliced ion imaging method to explore the dissociative ionization of molecular IBr under an 800 nm femtosecond laser field. By studying the angular distributions and measured KER of fragment ions, distinct ionization dynamical processes originating from various molecular orbitals have been identified. The findings indicate that the impact of different molecular orbitals can be discerned through the characteristics of the angular distribution. Furthermore, the differences in fragment ion yields are predominantly influenced by the charge distribution and ionization energy of the molecular fragments.

2. Experiment and Theory Calculation

Here, the DC-sliced ion velocity imaging system is briefly outlined [17,18]. Argon gas is utilized to transport IBr samples at a pressure of 2.5 atm, after which it is introduced into the source chamber. This chamber is regulated by a pulsed valve (General Valve, Parker, Cleveland, OH, USA) operating at a frequency of 100 Hz for a duration of 120~170 μs. The pulse width duration is calibrated in accordance with the quality of the sampled image to guarantee the clarity of the captured image. An 800 nm femtosecond laser, operating at a repetition rate of 1 kHz and with a pulse duration of 100 fs, is focused into the reaction chamber using a 400 mm focal length lens. Upon traversing the skimmer, the molecular beam enters the reaction chamber, where it interacts with a linearly polarized femtosecond pulse at the midpoint between the repeller and extractor plates of the ion lens. Electrodes are set at voltages of $U_{Repeller}$ = 2500 V, U_1 = 2220 V, U_2 = 2050 V, and U_3 = 0 V, optimized through ion trajectory calculations using SIMION 8.0 software. The electrode voltages also need to be adjusted to ensure that ions emitted with the same kinetic energy can be focused on the concentric ring positions of the collector. Fragment ions are detected by a dual micro-channel plate (MCP) coupled with the P47 phosphor screen, and sliced images are captured using a charge-coupled device (CCD) camera (PI-MAXII, Princeton Instrument, Trenton, NJ, USA). Each image is generated from 3000 laser shots. Time-of-flight (TOF) mass spectra are obtained using a digital oscilloscope (LeCroy Wave Pro) and a photomultiplier tube (H7732-11, Hamamatsu, Shizuoka, JP). The time sequence is regulated by a digital delay/pulse (DG535, Stanford Instrument, Sunnyvale, CA, USA).

Theoretical calculations were performed using the GAUSSIAN 09 software package [19]. Potential energy curves (PECs) were computed utilizing an aug-cc-pvtz basis set at the equation of motion coupled cluster (EOM-CCSD) level [20,21]. Frontier molecular orbitals (FMOs) were determined at the MP2 level with the DEF2TZVP basis set [22,23].

3. Results and Discussion

Figure 1 shows the obtained pseudo-color DC-sliced images of I^+ and Br^+ ions and the corresponding velocity distributions in the laser intensity of 3.0×10^{14} W/cm^2. The left panel presents a 512 × 512 pixel map depicting the ion distribution, with distinct ring

structures denoting varying ion ejection velocities. The distance of a ring from the center is positively correlated with the velocity of ion ejection; specifically, a greater distance results in an increased ion ejection velocity. Additionally, the intensity of the color of rings observed is indicative of the ion yield, with more vibrant colors representing higher yields. The right-hand side presents the normalized velocity distribution of fragment ions. The distribution exhibits multiple peaks, which are characterized by the application of a Gaussian function (the green dashed line) to model each peak. The fitting process involves adjusting the weights of the individual Gaussian functions and subsequently superimposing them (the red solid line) to align with the measured values (the black hollow circles). The peak value of each velocity distribution in the plot corresponds to the mean value (μ) of the Gaussian function, which is then multiplied by the respective ion mass to derive the KER value in eV. It should be noted that experimental errors are inherent in measurement and statistical data. Based on empirical evidence, it is posited that the acceptable error range for KER is within 10%. Generally, the lower kinetic energy fragment ions are attributed to the dissociation process of the parent molecular ion in the low valence state. The reason is that it is often generated at lower laser intensities, when the parent molecules are mostly ionized by MPI to form parent molecular ions, which then break chemical bonds to form fragment ions, and the fragments' KER is generally within the energy of a single photon. Higher kinetic energy fragmentation ions are often generated when the laser intensity is high, and multiple electrons can easily escape to form multi-charged parent ions, so the fragmentation ions tend to have higher kinetic energies under the action of the internal Coulomb potential. Considering that the fragment ions in the inner ring were collected at lower laser intensities and that the single photon energy of the 800 nm laser is 1.55 eV, we believe that the above fragment ions with kinetic energies lower than 1.0 eV originate from the dissociation process of the single-charged parent ion [24,25]. This study does not focus on analyzing fragment ions with higher kinetic energies, usually produced through a Coulomb explosion process, the specific dissociation dynamics are detailed in [26]. The latter phenomenon is associated with a multi-electron ionization process that involves the stretching of nuclear spacing, while the former does not require consideration of nuclear motion. Therefore, the examination of fragment ions exhibiting low KER values can complement the comprehension of strong field dynamics.

The dissociation pathways of molecular ions IBr^+ can involve either $IBr^+ \rightarrow I^+ + Br$ or $IBr^+ \rightarrow I + Br^+$. The I^+ ions exhibit two low-KER components at 0.05 and 0.23 eV, denoted as pathways $(1, 0)^a$ and $(1, 0)^b$ for convenience. The Br^+ ion displays two distinct KER components, specifically at 0.00 eV and 0.37 eV. The lower KER component is attributed to the ejection of an electron. And this electron is removed from the Ar_2 dimer rather than from the Br atom itself. Due to the long time (about picoseconds) required to first dissociate the Br atoms and then ionize them into Br^+ ions, this process does not occur within a femtosecond laser pulse. We suggest that Ar may have formed Ar_2 dimers, which were subsequently ionized to Ar_2^+ during the calibration of the laser intensity. According to the conservation of momentum principle, the kinetic energy of ion Ar_2^+ should approach 0 eV because the electron carries very little kinetic energy. Given that the mass-to-charge ratio of Ar_2^+ is equivalent to that of Br^+, the ion Ar_2^+ is observable in the DC-sliced images of fragment ion Br^+. To ensure clarity, the source of the Br^+ ion (0.37 eV) is identified as pathway (0, 1).

Table 1 presents the kinetic energies of the dissociation products associated with the aforementioned channels, with the kinetic energies of the neutral products derived from the principle of momentum conservation (indicated in italics). Given the significantly smaller mass of an electron compared to that of an atom or molecule, its contribution to the overall kinetic energy is considered negligible. In Table 1, the total kinetic energies of the channels $(1, 0)^a$, $(1, 0)^b$, and (0, 1) have been quantified as 0.13 eV, 0.59 eV, and 0.60 eV, respectively. It is noteworthy that the kinetic energies of the latter two channels exhibit a close resemblance, indicating a potential shared source stemming from a dissociative

mechanism. In order to make additional distinctions, it is essential to characterize these angle distributions of above channels.

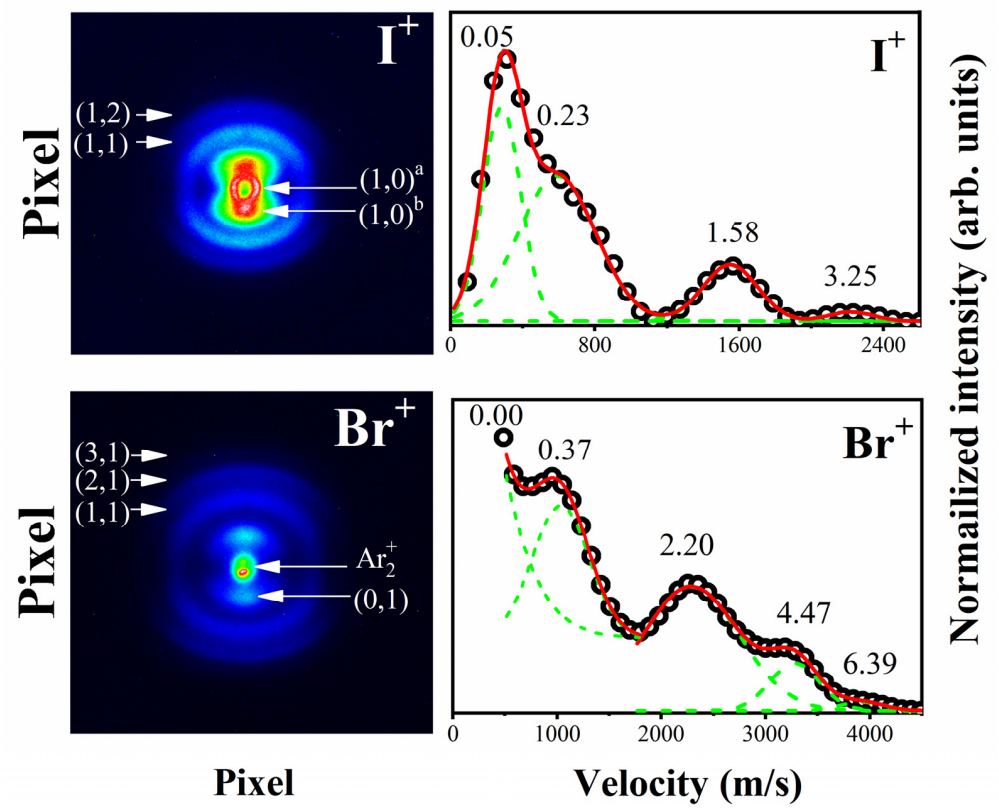

Figure 1. The pseudo-color DC-sliced images and velocity distributions of I^+ and Br^+ in the laser intensity of 3.0×10^{14} W/cm^2, respectively. The labels represent the KER values (eV) of the fragment ions, the red solid lines (—) represent the simulated distributions, the black hollow circles (○) represent the experimental data, and the green dashed lines (---) represent the single Gaussian function.

Table 1. The KERs of fragment ions and total KERs of channels are listed.

Channel	I^+ KER (eV)	Br^+ KER (eV)	Total KER (eV)
$(1, 0)^a$	0.05	*0.08* [1]	*0.13* [1]
$(1, 0)^b$	0.23	*0.36* [1]	*0.59* [1]
(0, 1)	*0.23* [1]	0.37	*0.60* [1]

[1] The italic numbers are calculated through momentum conservation.

Figure 2 presents the angular distribution of I^+ and Br^+ ions. In Figure 2a, I^+ ions from distinct channels exhibit varying distributions, with the ions from the pathway $(1, 0)^a$ displaying anisotropic characteristics perpendicular to the laser polarization direction (blue hollow circles), while those from the pathway $(1, 0)^b$ exhibit anisotropic features parallel to the laser polarization direction (red hollow squares). In Figure 2b, the angular distribution of Br^+ ions (green hollow circles) resembles that of I^+ ions from the pathway $(1, 0)^b$, showing anisotropic characteristics parallel to the laser polarization direction. We suggest that the observed differences reflect distinct underlying mechanisms of strong field dynamics. The first conjecture is that ionization occurs at different locations, i.e., electrons are removed from different molecular orbitals.

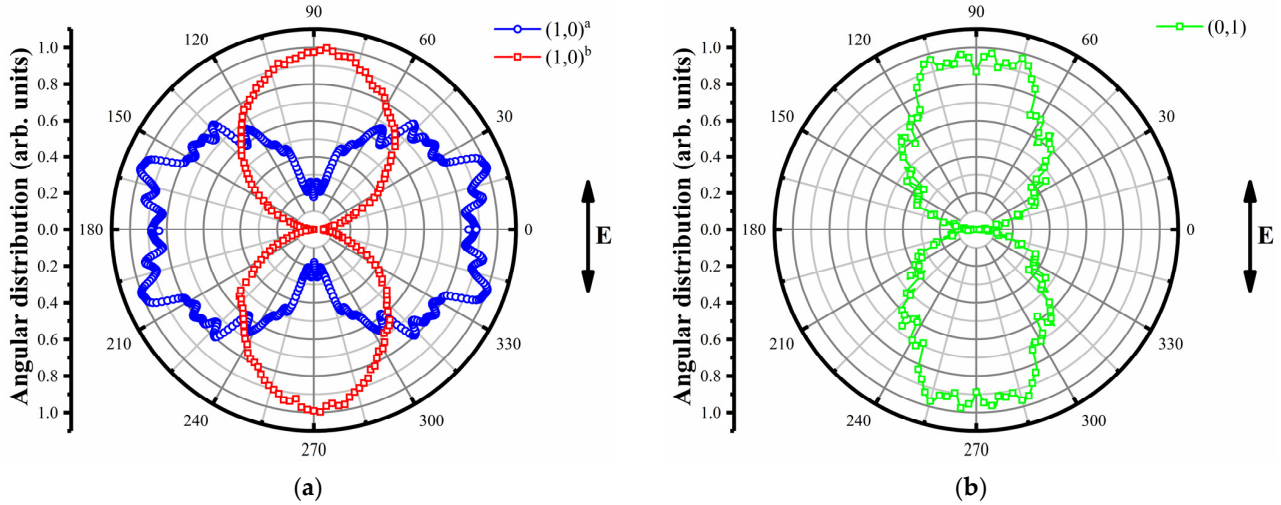

Figure 2. The angular distribution of fragment ions (**a**) I^+ and (**b**) Br^+ in the laser intensity of 3.0×10^{14} W/cm^2. The double arrows represent laser polarization.

Figure 3 displays various FMOs of neutral IBr, which were computed using the Gaussian 09 program at the MP2 level with the DEF2TZVP basis set. The electron configuration of the neutral IBr molecule is KK$(\sigma^*_u)^2(\sigma_g)^2\ (\pi_u)^2(\pi_u)^2(\pi^*_g)^2(\pi^*_g)^2$. The electron configurations of the two-energy degenerate HOMO orbitals are anti-bonding π^* orbitals and the two-energy degenerate HOMO-1 orbitals are bonding π orbitals. The HOMO-2 orbital is a σ_g orbital. The calculated vertical ionization potentials for the removal of one electron from these orbitals are 10.3 eV (HOMO orbitals), 13.0 eV (HOMO-1 orbitals), and 13.7 eV (HOMO-2 orbitals). The HOMO-3 orbitals are excluded from this analysis due to their high corresponding vertical ionization potentials (23.9 eV), making it improbable for the neutral IBr molecule to be excited to these states under the experimental conditions. Subsequently, potential energy curves (PECs) were computed to investigate the dissociation dynamics. Initially, the conformations of both the molecule and its parent ion were optimized at the MP2/def2TZV level. Subsequently, the bond lengths of the parent ion varied within the range of 1.5 to 5.0 Å. Following this, calculations were conducted to determine 20 excited states at the EOMCCSD/aug-cc-pvtz level. Finally, the potential energy curves for multiple excited states were obtained.

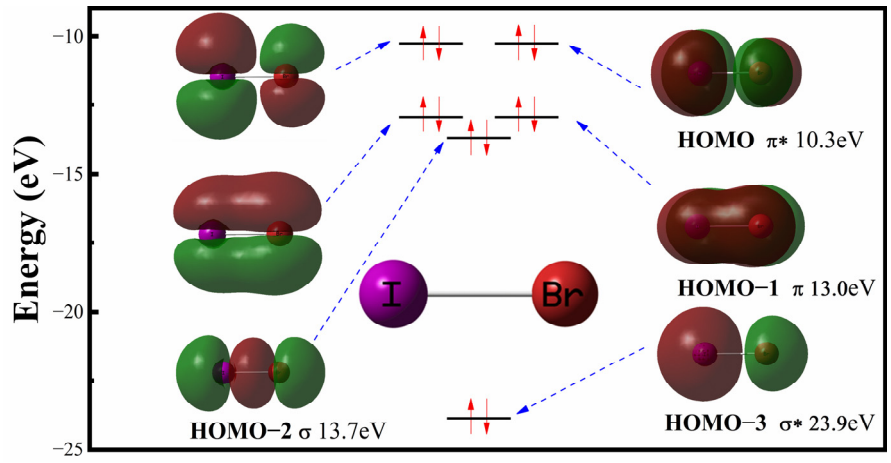

Figure 3. The calculated frontier molecular orbitals of IBr. The red arrows represent the different electron spin.

Figure 4 shows a variety of PECs representing ground and various excited states of IBr and IBr^+ ions, where G_0 and S_0 are the ground-state potential energy curves of the

parent molecules and ions, and S_4 and S_{13} are the potential energy curves of the fourth and thirteenth excited states of the parent ions, respectively. In the presence of a femtosecond laser field, the ionization process of IBr^+ is considered to be vertical ionization. Initially, ionization occurs at the equilibrium internuclear distance (R_e = 2.47 Å) of the neutral IBr molecule. Subsequently, the molecular ion experiences a dissociation process, resulting in the release of kinetic energy. The overall kinetic energy release linked to the dissociation pathway can be determined using Equation (1), where $\Delta E_{n,m}^{meas}$ represents the total KER, and $V_{n,m}$ represents the potential energy. In our analysis, we assume that dissociation initiates at the equilibrium nuclear separation and concludes at a nuclear separation of 5 Å. The difference between the two potential energies is the total energy released by the dissociation process.

$$\Delta E_{n,m}^{meas} = V_{n,m}(R_{ion}) - V_{n,m}(\infty)$$

First, we focused on pathways $(1, 0)^b$ and (0, 1). As shown in Figure 2, the distinct anisotropic angular distribution aligned with the laser polarization direction indicates the expulsion of an electron from the HOMO-2. This event can be explained through the following steps: Initially, the I-Br bond is oriented in the same direction as the polarization of the laser field, and ionization is facilitated by the removal of an electron from the HOMO-2, resulting in the formation of IBr^+ ions. Subsequently, a rapid dissociation process occurs, resulting in the splitting of IBr^+ into I^+ or Br^+ ions along the axis of the I-Br bond. Eventually, the dissociated fragment ions are distributed mainly along the laser polarization direction. As labeled in Table 1, the total kinetic energy produced by the two channels is observed to be between 0.59 and 0.6 eV. Considering the experimental error, the kinetic energy released from the excited state S_{13} is consistent with the experimental results. Therefore, it can be concluded that the two channels originate from the dissociation of excited state S_{13}. At this point, we are able to illustrate a comprehensive overview of the kinetic processes related to the two aforementioned channels, as indicated by the red arrows in Figure 4. Initially, an electron is removed from the HOMO-2. Following this, the resulting molecular ions are excited to the excited state S_{13}. Ultimately, this process results in dissociation, facilitating the experimental quantification of fragment ions.

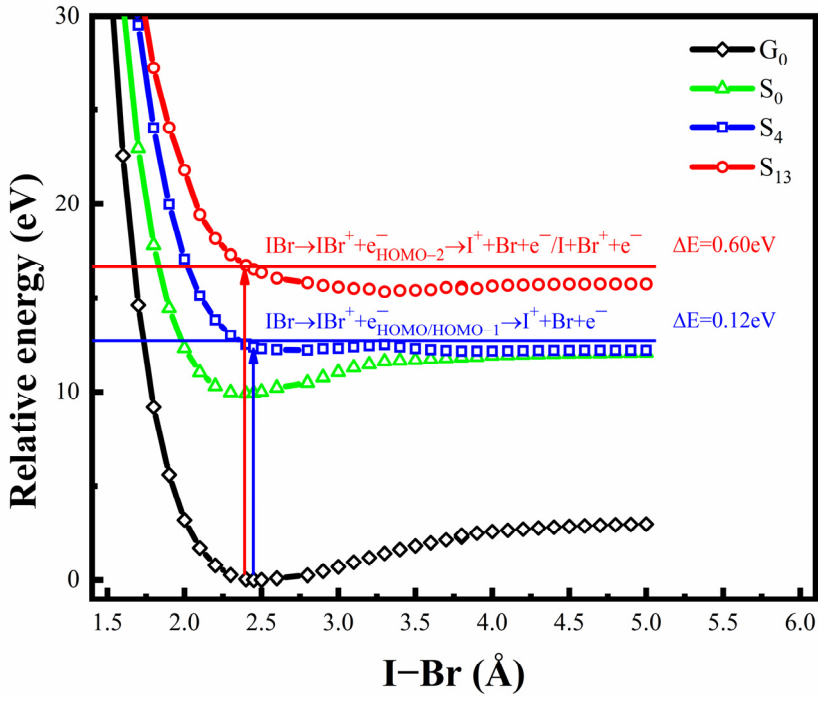

Figure 4. Calculated PECs of ground and several excited states of IBr and IBr^+ ions. The arrows represent the vertical excitation in the equilibrium internuclear distance (R_e) of neutral IBr molecule.

The DC-sliced images presented in Figure 1 indicate that the ion yield associated with pathway $(1, 0)^b$ is greater than that of pathway (0, 1). The primary difference between these two dissociation processes is attributed to the variation in charge distribution. Hence, the Natural Bond Orbital (NBO) charge distribution of IBr^+ was calculated, as shown in Figure 5. The result reveals that the I and Br atoms in IBr^+ exhibit a shared positive charge, with the I atom carrying a charge of +0.895 and the Br atom carrying a charge of +0.105. Upon the rupture of the I-Br bond, either I or Br loses the 'spare electron', resulting in pathway $(1, 0)^b$ or (0, 1). The determination of which fragment is more likely to lose the 'spare electron' depends on its ionization energy, which also influences the dissociation energy of the two pathways. The ionization energy of I (12.08 eV) is slightly lower than that of Br (13.65 eV), and the 'spare electron' is less I atom lost compared to the Br atom. Therefore, pathway $(1, 0)^b$ is more readily accessible than pathway (0, 1), so the former has a higher yield of fragment ions.

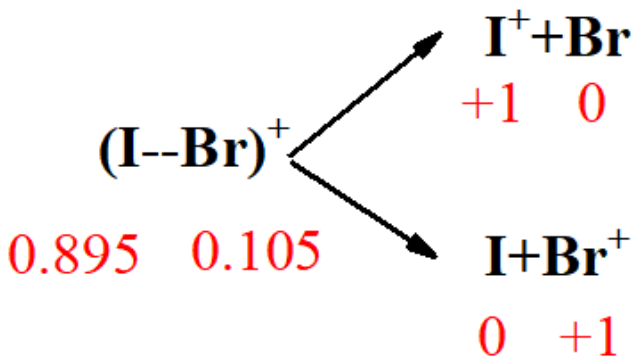

Figure 5. NBO charge distribution of IBr^+ ions and the charge assignment of the corresponding dissociation channels.

Then, we focus on pathway $(1, 0)^a$, which involves a more intricate dynamics process. As shown in Figure 2a, the angular distribution of the channel fragment ions is predominantly oriented perpendicular to the direction of the laser field polarization. We suggest that the stripped electrons should originate from the HOMO. The specific dissociative ionization process is as follows: First, the probability of ionization from the HOMO decreases when the laser is aligned either parallel or perpendicular to the I-Br bond. This decline can be explained by the diminished likelihood of electron distribution occurring in the direction of the laser's polarization. Subsequently, the rapid dissociation along the I-Br bond occurs, resulting in a negligible distribution of fragment ions in both parallel and perpendicular orientations relative to the laser polarization. However, there are more ions distributed in the perpendicular laser polarization direction ($0.8\sim0.9@0^\circ\pm15^\circ$) than in the parallel laser polarization direction ($0.2\sim0.4@90^\circ\pm15^\circ$). We believe that it is the fact that the electrons in HOMO-1 are also stripped off during the ionization process that leads to these differences. Unlike HOMO, the electron distribution of HOMO-1 is predominantly on both sides of the I-Br bond. When the laser is aligned parallel to the I-Br bond, the likelihood of ionization from the HOMO-1 decreases, resulting in a reduced number of fragment ions produced during the subsequent rapid dissociation process. Consequently, the angular distribution of these ions is expected to be diminished in the direction of laser polarization. Hence, the concurrent participation of the ionization processes originating from both orbitals promotes the overlap of the angular distribution of fragment ions, thereby demonstrating the features illustrated in Figure 2a. Recent research has shown that the ionization process of molecules in intense laser fields is significantly affected by the multi-orbital effect [27,28], which further supports the validity of the aforementioned hypothesis. The subsequent dissociation process is similar to the previous analyses, with the excited state S_4 releasing a kinetic energy of 0.12 eV, and taking into account the experimental error, we believe that the pathway $(1, 0)^a$ indeed originates from the dissociation of the excited state S_4. By now,

the dynamic processes associated with pathway (1, 0)[a] have been elucidated, as indicated by the blue arrow in Figure 4. Initially, an electron is extracted from either HOMO or HOMO-1. Subsequently, the molecular ions are excited to the excited state S_4. Ultimately, the dissociation process occurs, leading to the experimental measurement of fragment ions.

4. Conclusions

The dissociative ionization of the IBr molecule in an intense femtosecond laser field was investigated. The kinetic energy release and angular distribution of the fragment ions were measured and analyzed. It was determined that the variation in the angular distribution of I^+ ions along pathways (1, 0)[a] and (1, 0)[b] is primarily attributable to the distinct molecular orbitals from which electrons are ejected during the ionization process. In the scenario of path (1, 0)[a], the analysis suggests that the ionization process involves the participation of electrons from several molecular orbitals. Furthermore, for pathways (1, 0)[b] and (0, 1), the observed differences in fragment ions yield are predominantly influenced by the charge distribution and ionization energy of the molecular fragments. In contrast to previous studies, the present study reveals multi-orbital effects during dissociative ionization of heteronuclear diatomic molecules, thus extending the understanding of ultrafast dynamics in molecules under strong field excitation. Future investigations will focus on analyzing the proportion of orbital electrons involved in ionization processes to predict the angular distribution patterns observed in experiments.

Author Contributions: B.L. completed the experimental work and draft, and Z.L. finished part of theoretical calculation. The original experiment idea was proposed, and experiments were designed by Z.L. and B.L. submitted the final manuscript for publication. All authors have read and agreed to the published version of the manuscript.

Funding: This work has been partially supported by The Scientific Research Project for the Introduction of Talent of Yancheng Institute of Technology (No. xjr2021069), and The Natural Science Foundation of the Jiangsu Higher Education Institutions of China (No. 24KJB140020).

Institutional Review Board Statement: Not applicable.

Informed Consent Statement: Not applicable.

Data Availability Statement: Data are contained within the article.

Acknowledgments: Thanks to YanYang and Zhenrong Sun of East China Normal University for the experimental setup and technical support.

Conflicts of Interest: The authors declare no conflicts of interest.

References

1. Mainfray, G.; Manus, G. Multiphoton ionization of atoms. *Rep. Prog. Phys.* **1991**, *54*, 1333. [CrossRef]
2. Delone, N.B.; Krainov, V.P. Tunneling and barrier-suppression ionization of atoms and ions in a laser radiation field. *Phys.-Uspekhi* **1998**, *41*, 469. [CrossRef]
3. Ferray, M.; Huillier, A.L.; Li, X.F.; Lompre, L.A.; Mainfray, G.; Manus, C. Multiple-harmonic conversion of 1064 nm radiation in rare gases. *J. Phys. B At. Mol. Opt. Phys.* **1988**, *21*, L31. [CrossRef]
4. L'Huillier, A.; Lewenstein, M.; Salières, P.; Balcou, P.; Ivanov, M.Y.; Larsson, J.; Wahlström, C.G. High-order Harmonic-generation cutoff. *Phys. Rev. A* **1993**, *48*, R3433–R3436. [CrossRef] [PubMed]
5. Wu, Z.; Wu, C.; Liu, X.; Deng, Y.; Gong, Q.; Song, D.; Su, H. Double ionization of nitrogen from multiple orbitals. *J. Phys. Chem. A* **2010**, *114*, 6751–6756. [CrossRef] [PubMed]
6. Hatherly, P.; Stankiewicz, M.; Codling, K.; Frasinski, L.; Cross, G. The multielectron dissociative ionization of molecular iodine in intense laser fields. *J. Phys. B At. Mol. Opt. Phys.* **1994**, *27*, 2993. [CrossRef]
7. McKenna, J.; Suresh, M.; Srigengan, B.; Williams, I.; Bryan, W.; English, E.; Stebbings, S.; Newell, W.; Turcu, I.; Smith, J. Ultrafast ionization study of N_2 in intense linearly and circularly polarized laser fields. *Phys. Rev. A* **2006**, *73*, 043401. [CrossRef]
8. Zhang, J.; Li, Z.; Yang, Y. Multi-ionization of the Cl_2 molecule in the near-infrared femtosecond laser field. *RSC Adv.* **2020**, *10*, 332–337. [CrossRef]
9. Yao, H.-B.; Qu, Q.-W.; Zhang, Z.-H.; Wang, J.-W.; Gao, J.; Hu, C.-X.; Li, H.; Wu, J.; He, F. Multiphoton Ionization Reduction of Atoms in Two-Color Femtosecond Laser Fields. *Phys. Rev. Lett.* **2023**, *130*, 113201. [CrossRef]

10. Tang, Q.-B.; Shi, L.-K.; Zhang, K.; Kang, S.-J.; Li, Z.-F.; Wu, Y.-M.; Qin, L.-L.; Zhai, C.-Y.; Liu, A.-H.; Li, Y.-B. Electron dynamics of molecular frustrated double ionization driven by strong laser fields. *Commun. Theor. Phys.* **2023**, *75*, 035502. [CrossRef]
11. Pan, S.; Zhang, Z.; Xu, L.; Zhang, W.; Lu, P.; Ji, Q.; Lin, K.; Zhou, L.; Lu, C.; Ni, H.; et al. Manipulating Parallel and Perpendicular Multiphoton Transitions in H_2 Molecules. *Phys. Rev. Lett.* **2023**, *130*, 143203. [CrossRef] [PubMed]
12. Chan, C.K.; Brumer, P.; Shapiro, M. Coherent radiative control of IBr photodissociation via simultaneous (ω_1,ω_3) excitation. *J. Chem. Phys.* **1991**, *94*, 2688–2696. [CrossRef]
13. Jung, K.W.; Griffiths, J.; El-Sayed, M.A. Photofragment translational spectroscopy of IBr at 304 nm: Polarization dependence and dissociation dynamics. *J. Chem. Phys.* **1995**, *103*, 6999–7005. [CrossRef]
14. Lu, J.; Shao, F.; Fan, K. Coherent control of the photodissociation of CH_3I and IBr. *Chem. Phys. Lett.* **2000**, *329*, 461–468. [CrossRef]
15. Wrede, E.; Laubach, S.; Schulenburg, S.; Brown, A.; Wouters, E.R.; Orr-Ewing, A.J.; Ashfold, M.N.R. Continuum state spectroscopy: A high resolution ion imaging study of IBr photolysis in the wavelength range 440–685 nm. *J. Chem. Phys.* **2001**, *114*, 2629–2646. [CrossRef]
16. Ohmura, H.; Nakanaga, T.; Tachiya, M. Coherent control of photofragment separation in the dissociative ionization of IBr. *Phys. Rev. Lett.* **2004**, *92*, 113002. [CrossRef]
17. Yang, Y.; Fan, L.; Sun, S.; Zhang, J.; Chen, Y.; Zhang, S.; Jia, T.; Sun, Z. Dissociative double ionization of 1-bromo-2-chloroethane irradiated by an intense femtosecond laser field. *J. Chem. Phys.* **2011**, *135*, 064303. [CrossRef]
18. Hua, W.; Shian, Z.; Jian, Z.; Yan, Y.; Li, D.; Tianqing, J.; Zugeng, W.; Zhenrong, S. Observation of Hydrogen Migration in Cyclohexane under an Intense Femtosecond Laser Field. *J. Phys. Chem. A* **2015**, *119*, 2052–2057.
19. Frischet, M.J. *Gaussian 09, Revision D. 01*; Gaussian Inc.: Wallingford, CT, USA, 2009.
20. Stanton, J.F.; Bartlett, R.J. The equation of motion coupled-cluster method. A systematic biorthogonal approach to molecular excitation energies, transition probabilities, and excited state properties. *J. Chem. Phys.* **1993**, *98*, 7029–7039. [CrossRef]
21. Woon, D.E.; Dunning, T.H., Jr. Gaussian basis sets for use in correlated molecular calculations. III. The atoms aluminum through argon. *J. Chem. Phys.* **1993**, *98*, 1358–1371. [CrossRef]
22. Møller, C.; Plesset, M.S. Note on an approximation treatment for many-electron systems. *Phys. Rev.* **1934**, *46*, 618. [CrossRef]
23. Peintinger, M.F.; Oliveira, D.V.; Bredow, T. Consistent Gaussian basis sets of triple-zeta valence with polarization quality for solid-state calculations. *J. Comput. Chem.* **2013**, *34*, 451–459. [CrossRef]
24. Zhang, J.; Yang, Y.; Li, Z.P.; Sun, Z.R. Dissociative ionization of CH2Br2 in 800 and 400 nm femtosecond laser fields. *Chem. Phys. Lett.* **2017**, *685*, 151–156. [CrossRef]
25. Zhang, J.; Yang, Y.; Li, Z.P.; Zhang, S.A.; Sun, Z.R. Dissociative photoionization of 1,2-dichloroethane in intense near-infrared femtosecond laser field. *Chem. Phys. Lett.* **2017**, *667*, 238–243. [CrossRef]
26. Liu, B.; Li, Z.; Sun, Z.; Yang, Y. Multi-Electron Ionization and Coulomb Explosion of the IBr Molecule in the Near-Infrared Femtosecond Laser Field. *Appl. Sci.* **2023**, *13*, 13185. [CrossRef]
27. Pavičić, D.; Lee, K.F.; Rayner, D.M.; Corkum, P.B.; Villeneuve, D.M. Direct Measurement of the Angular Dependence of Ionization for N_2,O_2, and CO_2 in Intense Laser Fields. *Phys. Rev. Lett.* **2007**, *98*, 243001. [CrossRef]
28. McFarland, B.K.; Farrell, J.P.; Bucksbaum, P.H.; Gühr, M. High Harmonic Generation from Multiple Orbitals in N_2. *Science* **2008**, *322*, 1232–1235. [CrossRef]